Self-Assembly of Heme A and Heme B in a Designed Four-Helix Bundle: Implications for a Cytochrome *c* Oxidase Maquette[†]

Brian R. Gibney,[‡] Yasuhiro Isogai,[‡,§] Francesc Rabanal,[‡] Konda S. Reddy,[‡] Anne M. Grosset,[‡]
Christopher C. Moser,[‡] and P. Leslie Dutton*[,‡]

*The Johnson Research Foundation, Department of Biochemistry and Biophysics,
University of Pennsylvania, Philadelphia, Pennsylvania 19104, and Biophysical Chemistry Laboratory,
The Institute of Physical and Chemical Research (RIKEN), Wako, Saitama 351-01, Japan*

ABSTRACT: Heme A, a prosthetic group of cytochrome *c* oxidase [EC 1.9.3.1], has been introduced into two *de novo* designed four helix bundle proteins, [H10A24]$_2$ and [H10H24]$_2$, known to bind 2−4 equiv of heme B, respectively [Robertson, D. E., Farid, R. S., Moser, C. C., Mulholland, S. E., Pidikiti, R., Lear, J. D., Wand, A., J., DeGrado, W. F., and Dutton, P. L. (1994) *Nature 368*, 425−432]. [H10A24]$_2$, {[*Ac*-CGGGELWKL·**H**EELLKK·FEELLKL·AEERLKK·L-*CONH*$_2$]$_2$}$_2$, binds two heme A molecules per four-helix unit via bis-histidine ligation at the 10,10′ positions with measured K_d values of <0.1 and 5 nM, values much lower than those measured for heme B (K_d values of 50 and 800 nM). The heme A-protein complex, [heme A−H10A24]$_2$, exhibits well-defined absorption spectra in both the ferric and ferrous states, and an electron paramagnetic resonance spectrum characteristic of a low spin heme in the ferric form. A single midpoint redox potential (E_{m8}) was determined for [heme A−H10A24]$_2$ at −45 mV (vs SHE), which is significantly higher than that of the protein bound heme B (−130 and −200 mV). The observation of a single midpoint redox potential for [heme A−H10A24]$_2$ and a pair of midpoints for [heme B−H10A24]$_2$ indicates that the di-α-helical monomers are oriented in an anti topology (disulfides on opposite sides of bundle) in the former (lacking heme-heme electrostatic interaction) and syn in the latter. A mixture of global topologies was indicated by the potentiometric titration of the related [heme A−H10H24]$_2$ which possess two distinct reduction potentials of +41 (31%) and −65 mV (69%). Self-assembly of the mixed cofactor {heme A−heme B−[H10A24]$_2$} was accomplished by addition of a single equivalent of each heme A and heme B to [H10A24]$_2$. The single midpoint redox potential of heme B, E_{m8} = −200 mV, together with the split midpoint redox potential of heme A in {heme A−heme B−[H10A24]$_2$}, E_{m8} = +28 mV (33%) and −65 mV (67%), indicated the existence of both syn and anti topologies of the two di-α-helical monomers in this four helix bundle. Synthesis of the mixed cofactor [heme A−heme B−H10H24]$_2$ was accomplished by addition of a 2 equiv of each heme A and heme B to [H10H24]$_2$ and potentiometry indicated the pair of hemes B resided in the 10,10′ sites and heme A occupied the 24,24′ sites. The results indicate that heme peripheral structure controls the orientation of the di-α-helical monomers in the four-helix bundle which are interchangeable between syn and anti topologies. In the reduced form, [heme A−H10A24]$_2$, reacts quantitatively to form [carbonmonoxy-heme A−H10A24]$_2$ as evidenced by optical spectroscopy. The synthetic [heme A−H10A24]$_2$ can be enzymatically reduced by NAD(P)H with natural reductases under anaerobic conditions, and reversibly oxidized by dioxygen to the ferric form.

The design of minimalist peptides that assemble into well-defined structural units (*1*, *2*) and incorporate redox cofactors representing simplified redox protein structures, *maquettes* (*3*), of much more elaborate natural counterparts is now proving feasible. The current stage of development offers exploration into the assembly of more than one different cofactor into the same protein structure as is common in many redox proteins and oxidoreductase enzymes. Already we have successfully incorporated hemes with iron−sulfur clusters (using differential ligation motifs) (*4*), zinc porphyrins (*5*), flavins (*6*), or a coproporphyrin dimer (using covalent attachment) (*7*). Here we attempt to self-assemble two members of the same class of cofactor: heme A, well-known as a prosthetic group of oxidases (*8*) and heme B (ferric protoporphyrin IX), ubiquitous in cytochromes, oxygenases and oxidases (*9*, *10*). Figure 1 shows that heme A differs from heme B in peripheral porphyrin architecture; a formyl group replaces the methyl group at position one and a farnesyl side chain substitutes for the vinyl group at position eight. Additionally, the equilibrium midpoint redox potential (E_{m8} = −120 mV) of bis-histidine heme A (*11*, *12*) is
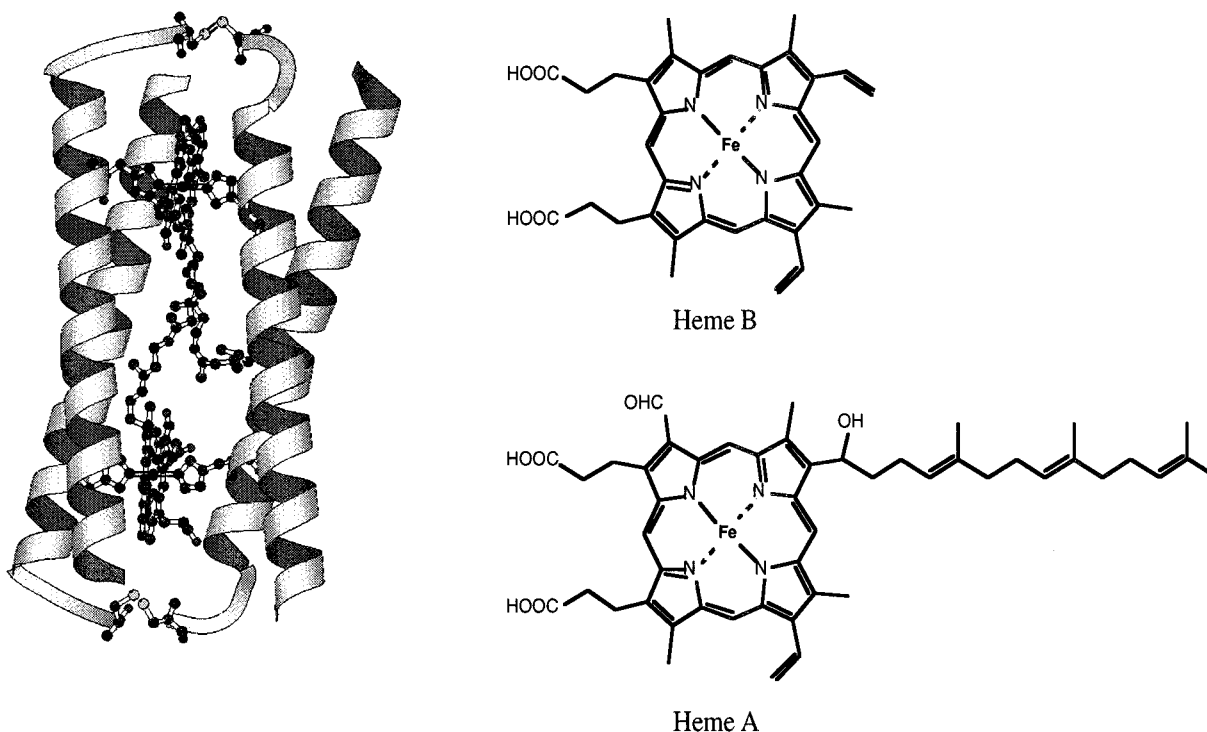
Heme B

Heme A

FIGURE 1: Molecular model of a structure of the anti-[heme A−H10A24]$_2$ consistent with the experimental data shown with the chemical structures of heme B and heme A for comparison. For clarity, only the cysteine and histidine side chains and the heme A are shown.

significantly higher than bis-histidine heme B (E_{m8} = −235 mV) (*13*). Thus, both electronic and steric differences particular to the two porphyrin architectures used are expected to modulate the heme-peptide interactions (heme affinity, reduction potential and global topology of the tetra-α-helical bundle scaffold). We expect that basic investigations using this constructive approach will lead to a deeper understanding of how native proteins organize the redox centers and establish their in situ properties to form a foundation toward the greater challenge of designing a functional enzyme.

We have chosen two related synthetic α-helical peptides known to bind heme B; *Ac*-CGGGELWKL·**H**EELLKK· FEELLKL·AEERLKK·L-*CONH*$_2$, here called H10A24, and *Ac*-CGGGELWKL·**H**EELLKK·FEELLKL·**H**EERLKK· L-*CONH*$_2$, here called H10H24, for ligation of heme A. After the disulfide bond formation by oxidation of the N-terminal cysteine thiols, the resulting 62-residue, di-α-helical peptides {generically (α-S−S-α)} spontaneously self-assemble into four-helix bundles {(α-S−S-α)$_2$} in aqueous solution. Figure 1 shows that two heme binding site are formed in [H10A24]$_2$ (four in [H10H24]$_2$) from the histidines at position 10 and 10′ (10,10′ and 24,24′ in [H10H24]$_2$) (*2*). The affinity of [H10A24]$_2$ for heme A is quantitated and the resultant spectroscopic, electrochemical and structural properties of bound heme A are described in comparison with [heme B−H10A24]$_2$, [heme A−H10H24]$_2$ and the native cytochrome A of cytochrome *c* oxidase. Self-assembly of mixed cofactor maquettes, containing both heme B and heme A, provides heme A−heme B−[H10A24]$_2$ and [heme A−heme B−H10H24]$_2$ whose distinct electrochemistry is used to derive the global peptide topology. The reaction of the synthetic [heme A−H10A24]$_2$ and [heme B−H10A24]$_2$ with native enzymes and with molecular oxygen are also described in functional aspects.

EXPERIMENTAL PROCEDURES

Chemicals and Solvents. Pyridine, acetic anhydride, diethyl ether, trifluoroacetic acid, and hemin ([iron(protoporphyrin IX)Cl]) were obtained from the Aldrich Chemical Co. (Milwaukee, WI). Ethanedithiol was purchased from Fluka (Ronkonkoma, NY). NovaSyn PR-500 resin was purchased from Calbiochem-Novabiochem (La Jolla, CA). Fmoc-protected amino acid pentafluorophenyl esters were purchased from PerSeptive Biosystems (Framingham, MA) with the exception of Fmoc-L-Arg(Pmc)-OPfp[1] which was obtained from Bachem (King of Prussia, PA). Spinach ferredoxin-NADP reductase (EC 1.18.1.2) and diaphorase (lipoyl dehydrogenase; EC 1.8.1.4) from *Clostridium kluyveri* were obtained from Sigma (St. Louis, MO) and used without further purification. All other chemicals and solvents were of the highest available grade and were used without further purification.

Peptide synthesis. All peptides were synthesized by solid-phase methodology at 0.2 mmol scale using standard Fmoc/ ^{t}Bu chemistry as described previously (*2*). The purity and identity of each peptide were confirmed by analytical HPLC and mass spectrometric analysis. The peptide concentration in aqueous solution was determined by UV absorption of the Trp residue using ϵ_{280} = 5700 mol^{-1} cm^{-1} helix^{-1}.

Circular Dichroism Spectropolarimetry: CD spectra were recorded on an AVIV 62DS spectropolarimeter using rectangular quartz cells of 0.2 and 1.0 cm path length. Thermal control was maintained by a thermoelectric module

with a Neslab CFT-33 refrigerated recirculating water bath as a heat sink. Peptide concentrations were between 2 and 5 μM as determined spectrophotometrically using $\epsilon_{280} = 5700$ mol^{-1} cm^{-1} helix^{-1} for Trp.

Solution Molecular Weight Determination: Gel filtration chromatography was performed on a Beckman System Gold HPLC system using a Supelco Sigmachrom GFC-100 column (7.5 × 300 mm) equilibrated with 10 mM Tris-HCl, pH 8.0, 200 mM NaCl at a flow rate of 0.5 mL/min.

Heme A Isolation. Heme A was prepared from beef heart by acid−acetone extraction and aqueous-ether phase partitioning (*14*), and finally purified by reversed-phase C$_{18}$ HPLC using water-acetonitrile gradients containing 0.1% (v/v) trifluoroacetic acid. The identity of heme A was established by the visible absorption spectra of the ferrous pyridine hemochrome formed in an aqueous solution containing 100 mM NaOH and 20% pyridine by addition of sodium dithionite. Stock heme A solution concentrations were determined by the α band peak of the pyridine hemochrome using an extinction coefficient (ϵ) of 27 000 M^{-1} cm^{-1} at 587 nm (*15*).

UV−Vis Spectroscopy. UV−vis absorption spectra were measured with a Perkin-Elmer Lambda 2 spectrophotometer at ambient temperature using quartz cells of 0.2 and 1.0 cm path length unless otherwise noted. Spectral changes in the time range faster than minutes were measured with Beckman DU-7500 diode array spectrophotometer.

Heme A Affinity. To determine dissociation constants (K_d) for ligation of heme A, 5 μM, 1 μM, and 60nM solutions of peptide (50 mM Tris-HCl, pH 8.0, 100 mM NaCl) were titrated with a 750 μM stock solution of heme A in DMSO at 20 °C in subdued light. Incremental additions of 0.1−0.2 equiv of heme A were incubated with the peptide solution until no further changes in the UV−vis absorption spectra were observed; this typically took over 60 min. The K_d was obtained from the absorbance at 421 nM plotted against total heme A concentration fitted to bound heme A and free heme A amounts according to equations for two independent binding sites (*16*). The extinction coefficient of the γ-band maxima at 421 nm of the oxidized [heme A-H10A24]$_2$ was evaluated to be 80 000 M^{-1} cm^{-1} heme A^{-1} from the titration data.

EPR Spectroscopy. Electron paramagnetic resonance (EPR) spectroscopy was performed using a Bruker ESP300E spectrometer. Temperature control was maintained by an Oxford ESR 900 continuous flow cryostat interfaced with an Oxford ITC4 temperature controller. Frequency was measured by a Hewlett-Packard 5350B frequency counter. EPR parameters: sample temperature, 30K; microwave frequency, 9.449 GHz; microwave power, 1 mW; modulation frequency, 100 kHz; modulation amplitude, 20.0 G; time constant, 164 ms.

Redox Potentiometry. Potentiometric titrations (*17*) were performed at 20 °C in 10 mM Tris-HCl, pH 8.0, and 100 mM NaCl by measuring the absorption spectra with a Perkin-Elmer spectrophotometer. The ambient redox potential was adjusted by addition of sodium dithionite or potassium ferricyanide, and monitored with a MI-800-401 micro-redox electrode (Microelectrodes, Bedford, NH). The potential was measured against a Ag/AgCl reference electrode and reported in the text against standard hydrogen electrode. Equilibration between the electrode and the reaction mixture was facilitated
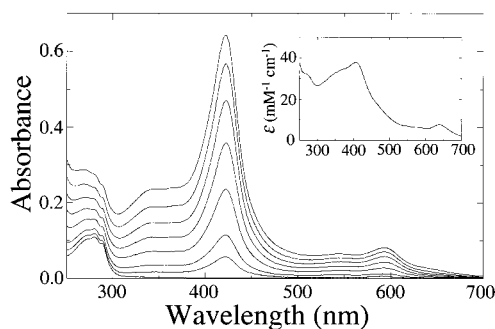

FIGURE 2: Introduction of heme A into [H10A24]$_2$ (5 μM four-α-helix bundle). UV−vis spectra of [H10A24]$_2$ after equilibration of stepwise addition of heme A at 0, 0.18 0.35, 0.7, 1.06, 1.41, 1.76, and 2.1 M equiv of [H10A24]$_2$ (for experimental details, see Experimental Procedures). (Inset) For comparison, the spectrum of heme A in the absence of peptide (50 mM Tris-HCl, pH 8.0, 100 mM NaCl).

with the redox mediators listed, as follows: 2,3,5,6-tetramethyl-*p*-phenylene diamine, 1,4-naphthoquinone, 1,2-naphthoquinone, phenazine ethosulfate, phenazine methosulfate, duroquinone, 2-hydroxy-1,4-naphthoquinone, anthroquinone-2-sulfonate, duroquinone, and 1,4-benzoquinone.

Molecular Modeling. Molecular modeling of peptide and heme-peptide complexes was carried out using a molecular modeling software Sybyl (TRIPOS Assoc. Inc., St. Louis, MO) on a Silicon Graphics Personal Iris or Indigo^2.

RESULTS

Introduction of Heme A. Figure 2 shows that in aqueous solution at 5 μM four helix bundle concentration, [H10A24]$_2$ gradually ligates two equivalents of heme A at room temperature as monitored by the visible absorption spectrum. Titration of a 1 mM solution of isolated, purified bovine heme A in DMSO into an aqueous solution of [H10A24]$_2$ with mild stirring results in slow incorporation of heme A into the peptide as evidenced by the development of the narrow γ-band with a maximum at 421 nm ($\epsilon = 8 \times 10^4$ M^{-1} cm^{-1}) (Table 1, Figure 2). Two independent K_d values (<0.1 and 5 nM) were evaluated with the titration data collected at 60 nM four helix bundle concentration (Figure 3A). The K_d values for [heme A−H10A24]$_2$ of <0.1 and 5 nM are significantly lower than the 50 and 800 nM K_d value previously reported for heme B in this peptide (*3*). Another difference is illustrated in Figure 3B, which shows that equilibration for the binding of heme A requires approximately 100 min, a rate some 40-fold slower than heme B incorporation into [H10A24]$_2$. Dithionite reduction of [heme A−H10A24]$_2$ yields an optical spectrum with the γ peak at 441 nm and the single peak at 598 nm in the α and β band region (Figure 4A). These spectra have profiles similar to those of cytochrome *c* oxidase (heme A + A$_3$), which show the γ peak at 420−425 nm in the oxidized form, and at 440−445 nm with the α peak at 595−607 nm in the reduced form (*18*, *19*).

Titration of one equivalent of heme B into solutions containing [H10A24]$_2$ with one equivalent of heme A incorporated result in formation of the mixed cofactor {heme A−heme B−[H10A24]$_2$} as monitored by the optical spectrum. In the oxidized state, {heme A−heme B−[H10A24]$_2$} yields an optical spectrum with the γ peak at 415 nm and peaks at 533 and 588 nm in the α and β band region (Figure 4A)

Table 1: Comparison of [heme B−H10A24]$_2$ and [heme A−H10A24]$_2$ Spectroscopy and Electrochemistry

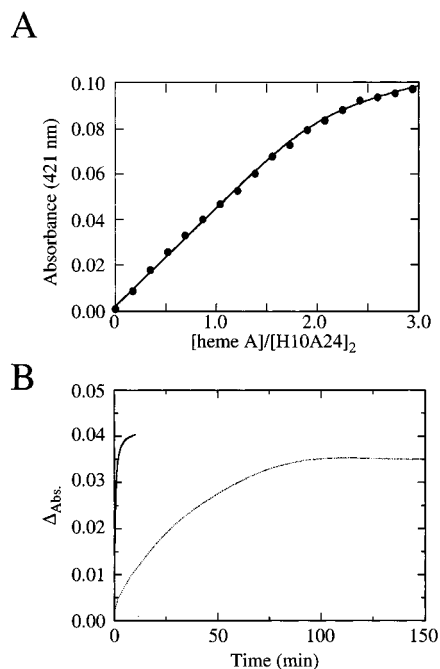|	[heme B−H10A24]$_2$	[heme A−H10A24]$_2$
λ_{max} (ϵ, mM^{-1} cm^{-1})		
oxidized	412 nm (120), 530 nm (13), 560 nm (11)	421 nm (80), 593 nm (6)
reduced	426 nm (160), 529 nm (17), 559 nm (28)	441 nm (91), 598 nm (13)
reduced−CO complex	418 nm (155), 536 nm (15), 564 nm (14)	433 nm (99), 600 nm (10)
K_d (nM)	50, 800	<0.1, 5
E_{m8} (mV vs SHE)	−100, −210	−45
EPR g-values	2.89, 2.24, 1.54	2.99, 2.26, 1.50

FIGURE 3: Thermodynamics and kinetics of heme A incorporation into [H10A24]$_2$. (A) The binding titration profile of [H10A24]$_2$ (60 nM four-α-helix bundle, 10 cm cuvette) with heme A. The absorbance at 421 nm is plotted against the concentration of heme A added per [H10A24]$_2$. A theoretical curve assuming two independent binding sites (14) with K_d values of <0.1 and 5 nM was fitted for the data as shown. (B) Relative kinetics of heme A (dotted line) and heme B (solid line) incorporation into [H10A24]$_2$.

FIGURE 4: Optical absorption spectra of (A) [heme A−H10A24]$_2$, (B) [heme A−H10H24]$_2$, (C) [heme A−heme B−H10A24]$_2$, and (D) [heme A−heme B−H10H24]$_2$ in the oxidized (solid line), dithionite-reduced (broken line), and reduced-CO-bound forms (dotted line) (50 mM Tris-HCl, pH 8.0, and 100 mM NaCl buffer).

similar to that observed for cytochrome ba_3 (416 and 537 nm). After dithionite reduction the optical spectrum at γ peak at 427 nm with a shoulder at 440 nm and peaks at 528, 558, and 591 nm in the α and β band region reminiscent of that observed for cytochrome ba_3 [427, 442 (sh.), 530, 560 and 611 nm] (20).

Protein Assembly. The effect of heme A ligation on the aggregation states of [H10A24]$_2$ and [H10H24]$_2$ was evaluated using size-exclusion chromatography. The parent peptides, [H10A24] and [H10H24], when dissolved in aqueous buffer elute with apparent molecular masses of 18.6 kDa (14.9 kDa calculated for the four helix bundle), on a column standardized with globular proteins, consistent with their formulation as four helix bundles. Stoichiometric addition of heme (either type) in 0.1 equiv increments with equilibration results in no change in the aggregation state of either bundle. However, the addition of excess amounts of heme A (>3 equiv to [H10A24]$_2$) results in an increase in the population of higher aggregation states (data not shown).

EPR Spectroscopy. The EPR spectrum of ferric [heme A−H10A24]$_2$ (not shown) shows a rhombic spectrum with the g_z, g_y, and g_x values at 2.99, 2.26, and 1.50, respectively,
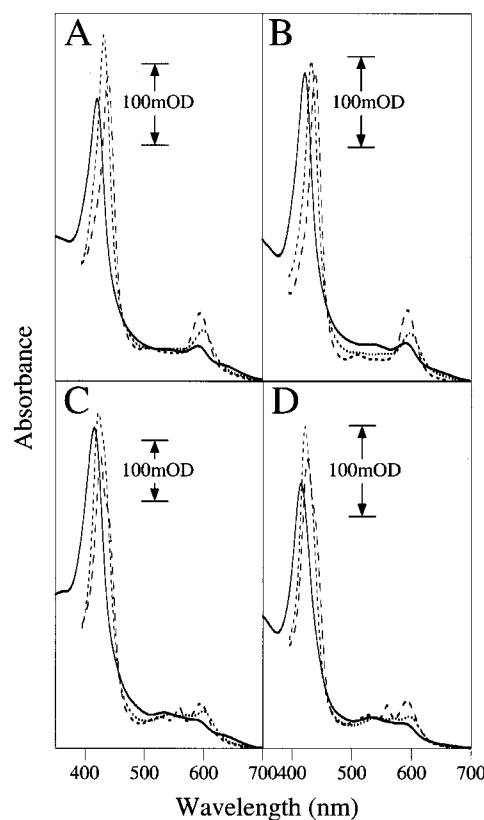
which are characteristic of a low spin, bis-histidine coordinated heme A iron. The spectrum is similar to those reported for other iron porphyrin species in [H10A24]$_2$ (g_z, g_y, g_x = 2.89, 2.24, 1.54, for heme B) (3, 21), except for slight shift of the g_z peak to the lower magnetic field. The EPR spectrum is strikingly similar to that of oxidized heme A of cytochrome c oxidase with g_z, g_y, g_x = 3.0, 2.2, 1.5 (22, 23).

Circular Dichroism. The effect of heme A incorporation on the secondary structure of [H10A24]$_2$ was evaluated by far-UV CD measurements. CD analysis of [H10A24]$_2$ with and without heme A in the UV region gave the mean residue ellipticity of −20 200 and −23 000 deg cm^2 dmol^{-1} at 222 nm, which indicate the helical contents of 63 and 70%, respectively, based on an ellipticity of −32 000 deg cm^2 dmol^{-1} for 100% helicity (24). The apparent decrease in the helical content upon heme A incorporation may be due to partial perturbation of the secondary structure by introduction of the bulky side chain of heme A to the hydrophobic interface or complications due to heme A CD bands in this spectral region.
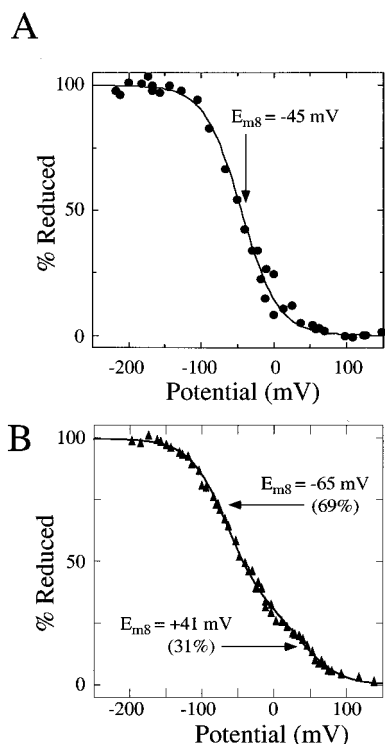
A

B

FIGURE 5: Potentiometric titration of (A) [heme A−H10A24]$_2$ and (B) [heme A−H10H24]$_2$. The reduced fraction of the bound heme A is plotted against ambient redox potential, which is indicated against standard hydrogen electrode. The shown Nernst curves (*n* = 1) were fitted to the data with a resultant midpoint redox potential of −45 mV (*n* = 1) for [heme A−H10A24]$_2$ and two components at −65 mV (69%) and +43 mV (31%) for [heme A−H10H24]$_2$.

Redox Potentiometry. Two Hemes A in [H10A24]$_2$. The electrochemical redox potentials of two bound hemes A in [H10A24]$_2$ were determined by monitoring the changes in the γ and α bands of the absorption spectra as a function of redox potential (Figure 5A). The redox titration of [heme A−H10A24]$_2$ shows the single component with a midpoint (E_{m8}) of −45 ± 10 mV. This contrasts sharply with the results from two bound hemes B in [H10A24]$_2$ which display two distinct states with midpoints at −200 and −130 mV, indicating electrostatic interaction between the hemes (*3*) in a syn bundle topology. The single electrochemical component in [heme A−H10A24]$_2$ suggest the overall topology of [heme A−H10A24]$_2$ and [heme B−H10A24]$_2$ are different; the addition of two hemes A induces [H10A24]$_2$ to adopt an anti global topology (loop regions on opposite sides of the bundle). Furthermore, incorporation of two hemes A into [H10S24]$_2$, known to be in the anti global topology in the apo and diheme B states (*40*), results in a maquette with an identical reduction potential (E_{m8}) of −45 mV ± 10 mV, demonstrating the electrochemical equivalence of the anti topology bundles, [heme A−H10S24]$_2$ and [heme A−H10A24]$_2$.

Two Hemes A in [H10H24]$_2$. Figure 5B shows a similar potentiometric titration of two hemes A in [H10H24]$_2$, a protein potentially able to bind four hemes at the pair of 10,10′ and 24,24′ positions. The [heme A−H10H24]$_2$ redox titration shows two components with midpoints (E_{m8}) of +41 ± 10 and −65 ± 10 mV in a ratio of ∼3:7 indicating a mixture of protein topologies. The electrochemical data suggest a minor syn bundle topology component with
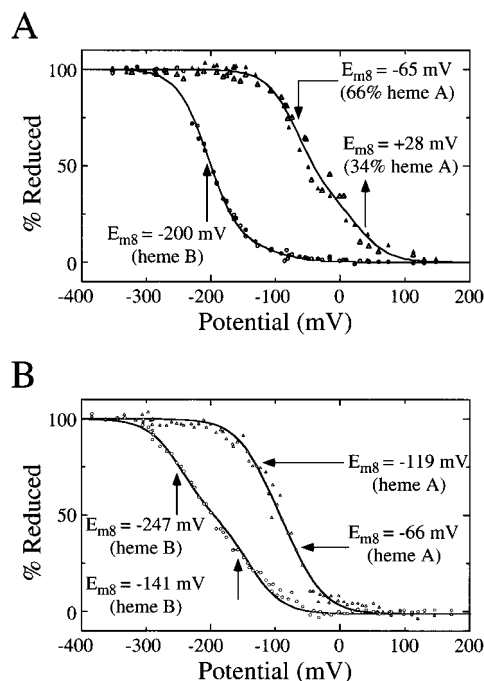
A

B

FIGURE 6: Potentiometric titrations for the mixed cofactor (heme A−heme B−[H10A24]$_2$) and ([heme A−heme B−H10H24]$_2$). The reduced percentage of the bound heme A and heme B are plotted against ambient redox potential (vs SHE). The Nernst curve (*n* = 1) with two components, shown, was fitted to the data with midpoint redox potentials of −200 mV for heme B and two components −65 mV (66%) and +28 mV (34%) for heme A in (heme A−heme B−[H10A24]$_2$). The measured midpoint redox potentials for ([heme A−heme B−H10H24]$_2$) are −247 and −141 mV for heme B and −119 and −66 mV for heme A.

interheme electrostatic interaction of 106 mV with the majority of the bundles being in an anti bundle topology.

One Heme A and One Heme B in [H10A24]$_2$. The redox titration of {heme A−heme B−[H10A24]$_2$} shown in Figure 6A indicates a single component for the heme B (monitored by $\Delta_{Abs.559−595}$) at −200 mV and two components for the heme A (monitored by $\Delta_{Abs.620−595}$) at −65 and +28 mV in a 2:1 ratio indicating a mixture of protein topologies. The electrochemical interaction energy of 93 mV is intermediate between that observed for [heme A−H10H24]$_2$ (106 mV) and [heme B−H10A24]$_2$ (70 mV).

Two Hemes A and Two Hemes B in [H10H24]$_2$. Figure 6B shows the redox titration of [heme A−heme B−H10H24]$_2$ with split heme B (−247 and −141 mV) and heme A (−119 and −65 mV) reduction potentials. The splitting of both sets of heme redox potentials indicate adjacent hemes are of the same type.

Reactivity with Exogenous Ligands. Ferrous-[heme A−H10A24]$_2$, ferrous-[heme A−H10H24]$_2$, ferrous-{heme A−heme B−[H10A24]$_2$}, and ferrous-[heme A−heme B−H10H24]$_2$ show quantitative reactivity with carbon monoxide (1 atm) to generate the ferrous−CO complexes. The ligation of CO with requisite histidine displacement is evidenced by the α peak shifting to a longer wavelength (601 nm as shown for ferrous−[CO−heme A−H10A24]$_2$ in Figure 4A) as is observed with other heme A compounds with nitrogenous ligands (*25, 26*), whereas it shifts to a shorter wavelength in heme A$_3$ of cytochrome *c* oxidase.

Enzymatic Reduction and Oxidation by O$_2$. Potential functional aspects of [heme A−H10A24]$_2$ were investigated
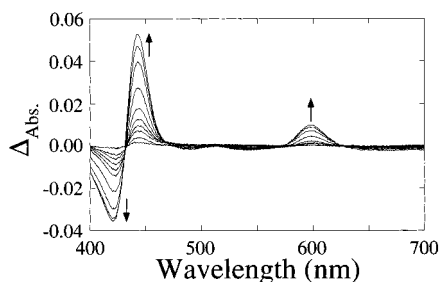
FIGURE 7: Enzymatic reduction of [heme A−H10A24]$_2$. [Heme A−H10A24]$_2$ (1 μM based on heme A concentration) was incubated with ferredoxin-NADPH reductase (1 μM) and NADPH (100 μM) under anaerobic conditions. The spectra were recorded at 0.5−30 min after the mixing and are displayed as difference spectra against that at 0 min.

by the use of native reductases for mediating electrons from NAD(P)H to the synthetic protein. Upon incubation of [heme A−H10A24]$_2$ with ferredoxin-NADPH reductase and NADPH under anaerobic conditions, [heme A−H10A24]$_2$ was observed to be reduced to the ferrous form in the minutes time scale (Figure 7). Control experiments demonstrated that the addition of NADPH or NADH to [heme A−H10A24]$_2$ or [heme B−H10A24]$_2$ without ferredoxin-NADPH reductase results in no reaction. Another reduction system examined, diaphorase with NADH, showed slower reduction activity (not shown). Addition of air to the reaction mixture resulted in facile oxidation of the [heme A−H10A24]$_2$ to the ferric form. The reoxidized [heme A−H10A24]$_2$ can be subsequently rereduced to the ferrous form by addition of NADPH, indicating that the reaction with O$_2$ is fully reversible. [Heme B−H10A24]$_2$ can be also be reversibly reduced enzymatically and reoxidized by molecular oxygen (not shown). The rate (k_{ox}) of the reoxidation of [heme B−H10A24]$_2$ was estimated at about 0.5 s^{-1} under air-saturated conditions at 20 °C, whereas k_{ox} for [heme A−H10A24]$_2$ was too fast to be determined (<0.05 s^{-1}) in the present experiments.

DISCUSSION

Spectral Similarities to Natural Heme A Proteins. The spectroscopic properties of [heme A−H10A24]$_2$ and [heme A−H10H24]$_2$ are remarkably similar their natural counterpart, heme A of cytochrome *c* oxidase. Additionally, the optical spectra of the two mixed cofactor maquettes, {heme A−heme B−[H10A24]$_2$} and [heme A−heme B−H10H24]$_2$, are reminiscent of cytochrome *ba*$_3$, a bacterial terminal oxidase, which contains a heme B in an analogous position to that of heme A in cytochrome *c* oxidase (*20*, *27*).

Heme A: Higher Affinity, Slower Incorporation than Heme B. The K_d values for heme A in [H10A24]$_2$ were <0.1 and 5 nM over 50-fold lower than those observed for heme B (50 and 800 nM). Another difference is observed in the kinetics of heme A insertion into the four helix bundle which are ∼40-fold slower than heme B incorporation; similar rates have been observed for heme A incorporation into a variety of proteins including hemoplexin and the H64V/V68H mutant of human myoglobin (*28*). Both effects are likely due to the hydrophobic farnesyl side chain of heme A. As much as 8 kcal/mol in transfer free energy (ΔG°_{tr}) may be obtained from the removal of the farnesyl tail from water into a low dielectric environment (*29*, *30*) so internalization

Scheme 1
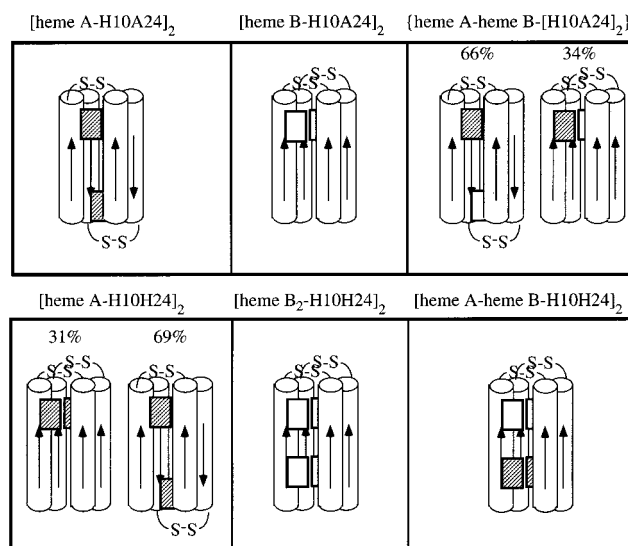
may override the fact that a cavity for the farnesyl tail was not explicitly designed into [H10A24]$_2$ which may account for the loss of some α-helical content.

Heme A: Higher Intrinsic Redox Potential Than Heme B, Further Elevated in a Hydrophobic Environment. The evaluated midpoint potential of [heme A−H10A24]$_2$ is −45 mV at pH 8.0 (Figure 5A) a value significantly higher than the −130 and −200 mV values observed for [heme B−H10A24]$_2$. Clearly, the replacement of a methyl group on heme B with an electron withdrawing formyl group on heme A preferentially stabilizes the ferrous state increasing the reduction potential of heme A (*31*) just as observed for the ketone substituted [methyl-2-oxomesoheme-H10A24]$_2$ whose E_{m8} value is −30 mV (*32*). The E_{m8} value of −45 for [heme A−H10A24]$_2$ is significantly higher than that of the heme A-histidine hemochrome (−120 mV) (*11*, *12*). Thus, localization of heme A within the hydrophobic environment of the synthetic four-helix bundle destabilizes the oxidized form with a net positive charge, compared with a water-accessible polar medium (*33*, *34*). However, and in consonance with this analysis, the potential of the [heme A−H10A24]$_2$ is much lower than those of the membrane bound hemes A in cytochrome *c* oxidase (+200 and +380 mV) (*19*, *35*) and heme A of cytochrome *ba*$_3$ (+356 mV) (*36*). The high potential of the native hemes A relative to [heme A−H10A24]$_2$ is due to a combination of factors which may be utilized in the future design of oxidase maquettes, including (1) the highly hydrophobic environment around the heme, (2) the hydrogen bond/ion pair formation of the formyl and one of the propionate side chains with two Arg residues in cytochrome *c* oxidase (*37*, *38*), and (3) the electrostatic interaction between the adjacent hemes A (*5*).

Redox Potentials, Charge Interactions, and Global Protein Topology. The observation of two distinct electrochemical states due to heme B−heme B charge interaction (ΔE_m = 70 mV) in the hydrophobic core of [heme B−H10A24]$_2$ indicated that the two di-α-helical units are positioned in a syn topology with the disulfide links at the same ends of the bundle (*2*) with a modeled Fe-to-Fe distance of 13 Å (Scheme 1). This syn topology was later confirmed when a single coproporphyrin probe appended to each di-α-helix monomer formed a cofacial dimer in the four-α-helix bundle

(*39*) and when the two bound protohemes III in [H10A24]$_2$ assumed inequivalent coordination states (*21*). However, in the present work with [heme A−H10A24]$_2$, inequivalent electrochemical states were not detected (Figure 5A) and the lack of an observable electrochemical interaction between the two bound heme A moieties in [heme A−H10A24]$_2$ is most consistent with an anti configuration in which models suggest an Fe-to-Fe distance of 26 Å would be expected (Figure 1, Scheme 1). The conversion of the syn dimer (loop regions on the same end) to the anti dimer (loop regions on opposite ends) is possibly due to steric effects of the long side chain of heme A analogous to the observed conversion of [H10A24]$_2$ from syn to anti upon a single amino acid modification, [H10S24]$_2$ (*40*).

In contrast to [heme A−H10A24]$_2$, the bound heme A moieties in [heme A−H10H24]$_2$ clearly possess a split in the heme A reduction potentials (E_{m8} = −65 and +43 mV, ΔE_m = 108 mV) indicating the presence of two distinct heme A electrochemical environments due to differences in bundle topology, as indicated in Scheme 1. The minor component of heme A bound to [heme A−H10H24]$_2$ has a raised E_{m8} value (+43 mV) due to heme−heme charge interaction in the syn bundle topology. The observed splitting in the E_m values due to heme-heme electrostatic interactions in the maquette are analogous to those observed between heme A and heme A$_3$ in cytochrome *c* oxidase and first proposed to be due to heme−heme electrostatic interactions by Wikström et al. (*41*). The presence of the adjacent oxidized heme A (net +1 charge) in the hydrophobic core results in elevation of the heme A potential by 108 mV, a value somewhat larger than the 70 mV interaction observed in [heme B−H10A24]$_2$ and within the 96−114 mV heme−heme interaction range observed in the cytochrome subunit of *Rhodopseudomonas viridis* reaction center (*42*). The reduction potential of the second heme A in a syn bundle topology is unaffected by the juxtaposed, reduced heme A (net neutral charge). The single reduction potential (−65 mV) of the major component of [heme A−H10H24]$_2$ indicates an anti bundle in which the bound heme A moieties have no electrochemical interaction with each other due to an Fe-to-Fe distance of ∼26 Å. The slightly lower reduction potential (−65 mV) of [heme A−H10H24]$_2$ with respect to [heme A−H10A24]$_2$ (−45 mV) may be a result of slight differences between the two peptides and solvent exposure.

The bound heme B in the mixed cofactor {heme A−heme B−[H10A24]$_2$} has a single reduction potential (E_{m8} = −200 mV) which is identical to that observed for the noninteracting heme B in [heme B−H10A24]$_2$ (E_{m8} = −200 mV) indicating it is in a similar electrochemical environment regardless of the identity of the other bound heme (heme B or heme A, reduced at these potentials). In addition, the observation of a single reduction potential attributable to heme B lacking a −130 mV component, indicates that single bundles containing two hemes B, [heme B−H10A24]$_2$, are not prevalent at equilibrium. In contrast to heme B, Figure 6A shows that the bound heme A moieties clearly do not possess a single reduction potential in {heme A−heme B−[H10A24]$_2$} (E_{m8} values of −65 and +28 mV in a 2:1 ratio). The raised E_{m8} value (+28 mV) of the minor component of heme A bound to {heme A−heme B−[H10A24]$_2$} indicates a syn bundle topology with a 93 mV interaction between the bound heme A and heme B (net positive charge) leaving the lower

reduction potential of the heme B unaffected by the adjacent, reduced heme A (net neutral charge). The electrochemical interaction energy, 93 mV, may be slightly higher relative to [H10A24]$_2$ due to decreased solvent exposure or partial charge compensation (*13*) within the hydrophobic core. The similarity of the reduction potentials (−65 and −200 mV) of the major component of {heme A−heme B−[H10A24]$_2$} with the reduction potentials of −45 mV (heme A) and −210 mV (heme B) measured for [heme A−H10A24]$_2$ and [heme B−H10A24]$_2$, respectively, indicates an anti topology in which the bound heme A and heme B have no electrochemical interaction. Thus, the two electrochemical states of the bound heme A in [heme A−H10H24]$_2$ and {heme A−heme B−[H10A24]$_2$} illustrates that incorporation of these heme cofactors have placed the bundle on the cusp between a syn and an anti topology (Scheme 1).

Figure 6B shows that the bound heme A moieties of the mixed cofactor [heme A−heme B−H10H24]$_2$ have reduction potentials (E_{m8} values) of −66 and −119 mV with reduction potentials of −141 and −247 mV for the bound hemes B. Both observed heme A−heme A and heme B−heme B electrochemical interactions (53 and 106 mV) indicate a global topology in which adjacent hemes are of the same type. The reduced electrochemical interaction energy (53 mV) and the lower reduction potentials of the heme A moieties, −119 mV is identical to the heme A-histidine hemochrome (−120 mV) at the same pH (*8, 9*), relative to [heme A−H10A24]$_2$ and [heme A−H10H24]$_2$ indicate significant exposure of heme A to solvent in this bundle. The similarity of the reduction potentials (−141 and −247 mV) of the bound hemes B and the 106 mV electrostatic interaction in [heme A−heme B−H10H24]$_2$ to the E_{m8} values of the hemes B in positions 10,10′ of [heme B-heme B−H10H24]$_2$ (−130 and −230 mV) and the observed 100 mV interaction energy of the bound hemes B in both indicates the efficient exclusion of solvent from the hydrophobic core in proximity to the hemes B. Furthermore, the small difference between the first heme A reduction potential in [heme A−heme B−H10H24]$_2$ (−66 mV) and the first heme B in [heme B−heme B−H10H24]$_2$ (−80 mV) is consistent with aqueous exposure leveling the intrinsic differences between heme A and heme B in this bundle with four bound hemes. The data are fully consistent with a syn topology with heme B at positions 10,10′ and heme A at position 24,24′ with increased solvent exposure toward the C-terminus.

In general, designed helical bundle structure is formed by projecting the hydrophilic residues toward the aqueous exterior and grouping the hydrophobic residues to reduce vacant space inside the bundle (*1, 43−45*). In the specific case of designed heme proteins, both monomeric and multimeric architectures have been utilized (*46−53*). In dimeric structures incorporating minimal hydrophobic cores (*54−57*), the difference in stability between the syn and anti topologies can be relatively small [<2 kcal/mol for a synthetic peptide related to [H10H24]$_2$ (*58*)], and easily reversed by simple structural or electrostatic perturbation. Such a change in topology is observed in the crystal structures of native ColE1 repressor of primer (ROP) (*59*) which is an anti topology coiled-coil and a single amino acid mutant (Ala31→Pro) (*60*) which assumes a bisecting U fold reminiscent of the designed α$_2$-D protein of Hill and

DeGrado (*61*). The electrochemical data presented provide an intrinsic probe of the global topology of these heme protein maquettes and indicate that bulky cofactors, e.g., heme A, are capable of controlling the global protein topology. In addition, the observed electrostatic interaction energy of adjacent hemes suggests that the placement of charged cofactors in close proximity at specific sites may destabilize the syn topology by electrostatic repulsion thereby generating preference for the anti topology. This is supported by the observed strong negative binding interaction between the bound heme A in another synthetic four-helix bundle in which the all parallel structure was fixed by a covalent bond between the loops of two helix-loop-helix monomers (Y. I., F. R., and P. L. D., unpublished data). Thus, even in this highly stable structure, the low interconversion barrier between syn and anti topologies can be overcome by the bound cofactors.

Functional Similarities to Natural Heme A Proteins. Ferric [heme A−H10A24]$_2$ (and [heme B−H10A24]$_2$) can be enzymatically reduced by ferredoxin-NADPH reductase with NADPH or diaphorase with NADH indicating the feasibility of interprotein electron transfer in these maquettes. Control experiments demonstrated the necessity for both the reductant [NAD(P)H] and the enzyme (ferredoxin-NADPH reductase or diaphorase) for reduction of the heme A and heme B in [H10A24]$_2$. The differential electron-transfer rates from NAD(P)H to [heme A−H10A24]$_2$ via the two enzymes studied is likely due to differences in both intrinsic enzymatic activity and enzyme−[heme A−H10A24]$_2$ interactions. The interaction of the designed [heme A−H10A24]$_2$ with natural reductases demonstrates interprotein electron transfer in a synthetic peptide system. In principle, these results illustrate the feasibility of inter-protein electron transfer by synthetic redox proteins similar to that found in many oxidoreductases.

Ferrous [heme A−H10A24]$_2$ (and [heme B−H10A24]$_2$), enzymatically or chemically formed, is rapidly and reversibly oxidized to the ferric form by ambient dioxygen. In this reaction, the hemes may reduce O_2 to O_2^- by an outer sphere mechanism without formation of the Fe(II)−O_2 complex (*62−64*). Alternatively, O_2 could bind to the heme iron (inner sphere mechanism) by replacing one of the histidine side chains, as an reaction intermediate to produce O_2^-. Because the ferrous [heme A−H10A24]$_2$ easily forms a complex with another exogenous diatomic, carbonmonoxide (Figure 4A), we tentatively favor the inner-sphere mechanism. More importantly, [H10A24]$_2$ protects the heme A (or heme B) within the hydrophobic core during these reactions preventing formation of the bis-μ-oxo Fe(III) species, which ensures the reversibility of the reaction with O_2. In contrast, almost all ferrous porphyrin compounds with nitrogenous ligands in isotropic solution are irreversibly oxidized by O_2 (*65*). The reversibility observed for [heme A−H10A24]$_2$ coupled with its demonstrated enzymatic reduction by NAD(P)H using native reductases indicates that the synthetic protein has an oxidase-like activity distinct from simple chemical compounds in isotropic solution. This reactivity was investigated to assess the feasibility of our initial effort to make a functional cytochrome *c* oxidase maquette and provides impetus for improvement in future designs.

Chemical Synthesis of Multicofactor Redox Proteins. After incorporation of a single equivalent of heme A into [H10A24]$_2$ addition of heme B provides for the assembly of the mixed cofactor {heme A−heme B−[H10A24]$_2$}. In this example, two distinct cofactors from the heme family can be incorporated into a single [H10A24]$_2$ by exploiting the binding stoichiometry, order of incorporation and the tight K_d values. Previously, we have examined the utilization of differential metal ligation motifs for the incorporation of both [4Fe-4S]$^{2+/+}$ clusters and hemes B into ferredoxin-heme maquettes and the use of covalent linkages to generate flavoheme maquettes (*66*). Clearly, future maquettes competent for the incorporation of catalytically active redox centers can make use of the NMR structure of a [H10H24]$_2$ variant (*67, 68*) and a variety of synthetic methods including covalent attachment chemistry, alternative ligation motifs and order of incorporation for their design and construction.

ACKNOWLEDGMENT

REFERENCES

1. Bryson, J. W., Betz, S. F., Lu, H. S., Suich, D. J., Zhou, H. X., O'Neil, K. T., and DeGrado, W. F. (1995) *Science 270*, 935−941.
2. Gibney, B. R., Rabanal, F., and Dutton, P. L. (1997) *Curr. Opin. Chem. Biol. 1*, 537−542.
3. Robertson, D. E., Farid, R. S., Moser, C. C., Mulholland, S. E., Pidikiti, R., Lear, J. D., Wand, A., J., DeGrado, W. F., and Dutton, P. L. (1994) *Nature 368*, 425−432.
4. Gibney, B. R., Mulholland, S. E., Rananal, F., and Dutton, P. L. (1996) *Proc. Natl. Acad. Sci. U.S.A. 93*, 15041−15046.
5. Sharp, R. E., Diers, J. W., Bocian, D. F., and Dutton, P. L. (1998) *J. Am. Chem. Soc. 120*, 7103−7104.
6. Sharp, R. E., Rabanal, F., Moser, C. C., and Dutton, P. L. (1998) *Proc. Natl. Acad. Sci. U.S.A. 95*, 10465−10470.
7. Rabanal, F., DeGrado, W. F., and Dutton, P. L. (1996) *J. Am. Chem. Soc. 118*, 473−474.
8. Babcock, G. T., and Wikstöm, M. (1992) *Nature 356*, 301−309.
9. Antonini, E., and Brunori, M. (1971) *Hemoglobin and Myoglobin in their Reactions with Ligands*, North-Holland, Amsterdam.
10. Chance, B., Estabrook, R. W., and Yonetani, T. (1966) *Heme proteins*, Academic Press, New York.
11. Vanderkooi, G., and Stotz, E. (1965) *J. Biol. Chem. 240*, 3418−3424.
12. Vanderkooi, G., and Stotz, E. (1966) *J. Biol. Chem. 241*, 3316−3323.
13. Shifman, J. M., Moser, C. C., Kalsbeck, W. A., Bocian, D. F., and Dutton, P. L. (1998) *Biochemistry 37*, 16815−827.
14. Tuppy, H., and Birkmayer, G. D. (1969) *Eur. J. Biochem. 8*, 237−243.
15. Berry, E. A., and Trumpower, B. L. (1987) *Anal. Biochem. 161*, 1−15.
16. Price, N. C., and Dwek, R. A. (1979) *Principles and Problems in Physical Chemistry for Biochemists*, 2nd ed., Oxford Universtiy Press, Oxford.
17. Dutton, P. L. (1978) *Methods Enzymol. 54*, 411−435.
18. Yonetani, T. (1961) *J. Biol. Chem. 236*, 1850−1856.
19. Wilson, D. F., and Erecinska, M. (1979) in *The Porphyrins* (Dolphin, D., ed.) Vol. VII, part B, pp 1−70, Academic Press, New York.
20. Zimmerman, B. H., Nitsche, C. I., Fee, J. A., Rusnak, F., and Münck, E. (1988) *Proc. Natl. Acad. Sci. U.S.A. 85*, 5779−5783.

21. Kalsbeck, W. A., Robertson, D. E., Pandey, R. K., Smith, K. M., Dutton, P. L., and Bocian, D. F. (1996) *Biochemistry 35*, 3429−3438.

22. van Gelder, B. F., and Beinert, H. (1969) *Biochim. Biophys. Acta 189*, 1−24.

23. Erecinska, M., Wilson, D. F., and Blaise, J. K. (1979) *Biochim. Biophys. Acta. 545*, 352−364.

24. Pace, C. N., Shirley, B. A., and Thompson, J. A. (1989) in *Protein Structure: A Practical Approach* (Creighton, T. E., Ed.) pp 311−330, IRL, Oxford.

25. Lemberg, R., Morell, D. B., Newton, N., and O'Hagan, J. E. (1961) *Proc. R. Soc. London, Ser. B 155*, 339−355.

26. Lemberg, R., Newton, N., and O'Hagan, J. E. (1961) *Proc. R. Soc. London, Ser. B 155*, 356−363.

27. Oertling, W. A., Surerus, K. K., Einarsdottir, O., Fee, J. A., Dyer, R. B., and Woodruff, W. H. (1994) *Biochemistry 33*, 3128−3141.

28. Felsch, J. S., Horvath, M. P., Gursky, S., Hobaugh, M. R., Goudreau, P. N., Fee, J. A., Morgan, W. T., Admiraal, S. J., Ikeda-Saito, M., Fujiwara, T., Fukumori, Y., Yamanaka, T., and Copeland, R. A. (1994) *Protein Sci. 3*, 2097−2103.

29. Warncke, K., and Dutton, P. L. (1993) *Proc. Natl. Acad. Sci. U.S.A. 90*, 2920−2924.

30. Warncke, K., Gunner, M. R., Braun, B. S., Gu, L., Yu, C.-A., Bruce, J. M., and Dutton, P. L. (1994) *Biochemistry 33*, 7830−7841.

31. Makino, R., and Yamazaki, I. (1972) *J. Biochem. 72*, 655−664.

32. Shifman, J. M., Gibney, B. R., Sharp, R. E., and Dutton, P. L. *Biochemistry* (in press).

33. Kassner, R. J. (1973) *J. Am. Chem. Soc. 95*, 2674−2677.

34. Churg, A. K., and Warshel, A. (1985) *Biochemistry 25*, 1675−1681.

35. Tsudzuki, T., and Wilson, D. F. (1971) *Arch. Biochem. Biophys. 145*, 149−154.

36. Scharf, B., Wittenberg, R., and Engelhard, M. (1997) *Biochemistry 36*, 4471−4479.

37. Tsukihara, T., Aoyama, H., Yamashita, E., Tomizaki, T., Yamaguchi, H., Shinzawa-Itoh, K., Nakashima, R., Yaono, R., and Yoshikawa, S. (1996) *Science 272*, 1136−1144.

38. Iwata, S., Ostermeier, C., Ludwig, B., and Michel, H. (1995) *Nature 376*, 660−669.

39. Grosset, A. M., Gibney, B. R., Rabanal, F., Moser, C. C., and Dutton, P. L. *Biochemistry* (manuscript in preparation).

40. Grosset, A. M., Rabanal, F., Farid, R. S., Roberston, D. E., DeGrado, W. F., Dutton, P. L. (1996) in *Peptides: Chemistry, Structure and Biology* (Kaumaya, T. P., and Hodges, R. S., Eds.) pp 573−574, Mayflower Scientific.

41. Wikström, M. K. F., Harmon, H. J., Ingledew, W. J., and Chance, B. (1976) *FEBS Lett. 65*, 259−277.

42. Gunner, M. R., and Honig, B. (1991) *Proc. Natl. Acad. Sci. U.S.A. 88*, 9151−9155.

43. Kamtekar, S., Schiffer, J. M., Xiong, H., Babik, J. M., and Hecht, M. H. (1993) *Science 262*, 1680−1685.

44. Lazar, G. A., Desjarlais, J. R., and Handel, T. M. (1997) *Protein Sci. 6*, 1167−1178.

45. Dahiyat, B. I., and Mayo, S. L. (1997) *Science 278*, 82−87.

46. Choma, C. T., Lear, J. T., Nelson, M. J., Dutton, P. L., Robertson, D. E., and DeGrado, W. F. (1994) *J. Am. Chem. Soc. 116*, 856−865.

47. Gibney, B. R., Rabanal, F., Reddy, K. S., and Dutton, P. L. (1998) *Biochemistry 37*, 4635−4643.

48. Benson, D. R., Hart, B. R., Zhu, X., and Doughty, M. B. (1995) *J. Am. Chem. Soc. 117*, 8502−8510.

49. Rau, H. K., DeJonge, N., and Haehnel, W. (1998) *Proc. Natl. Acad. Sci. U.S.A. 95*, 11526−11531.

50. Huffman, D. L., Rosenblatt, M. N., and Suslick, K. S. (1998) *J. Am. Chem. Soc. 120*, 6183−6184.

51. Isogai, Y., Ota, M., Fujisawa, T., Izuno, H., Mukai, M., Nakamura, H., Iizuka, T., and Nishikawa, K. (1999) *Biochemistry 38*, 7431−7443.

52. Rojas, N. R. L., Kamtekar, S., Simons, C. T., Mclean, J. E., Vogel, K. M., Spiro, T. G., Farid, R. S., and Hecht, M. H. (1997) *Protein Sci. 6*, 2512−2524.

53. Munson, M., Balasubramanian, S., Fleming, K. G., Nagi, A. D., O'Brien, R. O., Sturtevant, J. M., and Regan, L. (1996) *Protein Sci. 5*, 1584.

54. Betz, S. F., and DeGrado, W. F. (1996) *Biochemistry 35*, 6955−6962.

55. Brive, L., Dolphin, G. T., and Baltzer, L. (1997) *J. Am. Chem. Soc. 119*, 8598−8607.

56. Jiang, X., Bishop, E. J., and Farid, R. S. (1997) *J. Am. Chem. Soc. 119*, 838.

57. Gibney, B. R., Rananal, R., Skalicky, J. J., Wand, A. J., and Dutton, P. L. (1997) *J. Am. Chem. Soc. 119*, 2323−2324.

58. Gibney, B. R., Johansson, J. S., Rananal, R., Skalicky, J. J., Wand, A. J., and Dutton, P. L. (1997) *Biochemistry 36*, 2798−2806.

59. Banner, D. W., Kokkinidis, M., and Tsernoglou, D. (1987) *J. Mol. Biol. 196*, 657−675.

60. Glykos, N. M., Cesareni, G., and Kokkinidis, M. (1999) *Struct. Fold. Des. 7*, 597−603.

61. Hill, R. B., and DeGrado, W. F. (1998) *J. Am. Chem. Soc. 120*, 1138−1145.

62. Butler, J., Koppenol, W. H., and Margoliash, E. (1982) *J. Biol. Chem. 257*, 10747−10750.

63. Castro, C. E. (1978) in *The Porphyrins* (Dolphin, D., Ed.) Vol. V, part C, pp 1−27, Academic Press, New York.

64. Isogai, Y., Iizuka, T., and Shiro, Y. (1995) *J. Biol. Chem. 270*, 7853−7857.

65. James, B. R. (1978) in *The Porphyrins* (Dolphin, D., Ed.) Vol. V, part C, pp 207−302, Academic Press, New York.

66. Gibney, B. R., and Dutton, P. L. (2001) in *Adv. Inorg. Chem.* (Mauk, A. G., and Sykes, A. G., Eds.) Academic Press, New York, Vol 51, 409−455.

67. Skalicky, J. J., Gibney, B. R., Rabanal, F., Bieber-Urbauer, R. J., Dutton, P. L., and Wand, A. J. (1999) *J. Am. Chem. Soc 121*, 4941−4951.

68. Gibney, B. R., Rabanal, F., Skalicky, J. J., Wand, A. J., and Dutton, P. L. (1999) *J. Am. Chem. Soc. 121*, 4952−4960.